Hindawi
International Journal of Antennas and Propagation
Volume 2021, Article ID 5520268, 10 pages
https://doi.org/10.1155/2021/5520268

Research Article

Millimetre-Wave Metamaterial-Based Sensor for Characterisation of Cooking Oils

Suhail Asghar Qureshi,[1] **Zuhairiah Zainal Abidin**,[1] **Adel Yahya Isa Ashyap**,[1] **Huda A. Majid**,[1] **Muhammad Ramlee Kamarudin**,[1] **Ma Yue**,[2,3] **Mohd Syis Zulkipli**,[4] **and Jamel Nebhen**[5]

[1]*Advanced Telecommunication Research Center (ATRC), Faculty of Electrical and Electronics Engineering, Universiti Tun Hussein Onn Malaysia, Parit Raja, Batu Pahat 86400, Malaysia*
[2]*University of Chinese Academy of Sciences, Beijing 100049, China*
[3]*CAS Key Laboratory of FAST, National Astronomical Observatories, Chinese Academy of Sciences, Beijing 100101, China*
[4]*Pejabat Kesihatan Daerah Sepang, Jalan Salak, Sepang 43900, Malaysia*
[5]*Prince Sattam bin Abdulaziz University, College of Computer Engineering and Sciences, P.O. Box 151, Al-Kharj 11942, Saudi Arabia*

Correspondence should be addressed to Zuhairiah Zainal Abidin; zuhairia@uthm.edu.my

Received 6 January 2021; Revised 22 February 2021; Accepted 1 March 2021; Published 13 March 2021

Academic Editor: Ana Alejos

The characterisation of the cooking oils presents a significant challenge due to minor changes in their dielectric behaviour. In this paper, a new metamaterial-based sensor incorporating a split-ring resonator (SRR) with a microstrip transmission line is presented to characterise cooking oils. The design demonstrates metamaterial characteristics of negative permittivity and permeability simultaneously at the resonance frequency. Furthermore, its operation in the range of millimetre-wave frequencies can further enhance its sensitivity, especially for liquid materials. The sensor's novelty is the operation at millimetre-wave frequencies that offers a high shift in the transmission coefficient while operating at 30 GHz. The sensor's performance analysis is undertaken by using six MUTs with dielectric constants ranging from 0.126 to 4.47. The presented structure designed on $12 \times 8\,\text{mm}^2$ Rogers substrate offers a sensitivity of 1.12 GHz per unit change in dielectric constant. The phase's shift demonstrates a lower percentage error than the amplitude and linearly moves towards higher frequencies with the increase in dielectric constant and tangent loss of MUT. The designed sensor can be prominently useful for detecting liquids' chemical characteristics in chemistry and medicine fields.

1. Introduction

Each material has specific electrical properties, including permittivity, conductivity, tangent loss, and permeability. Microwave sensors are smart to measure these properties in biomedical, chemical, industrial, and electronic applications as they provide stable, high-quality, and highly sensitive sensing. The microwave sensors also reduce the cost of measurement and production. Various mechanisms of microwave sensors have been presented recently for dielectric characterisation of materials, including transmission line-based resonator [1, 2], cavity-based resonator [3, 4], oval wing resonator [5], and antenna-based resonator [6, 7]. Besides, the existing sensors have been presented for different applications such as material detection [8], label-free sensing of DNA [9], bacterial growth monitoring [10], and imaging of the breast [11]. In this regard, metamaterial resonators offer higher sensitivity than other microwave sensors and they have been reportedly found to sense small variation in EM (electromagnetic) properties of the sample [12]. As a result, metamaterial-based sensors have been presented for dielectric characterisation of ethanol and methanol [13], assessment of dielectric substrates [14], blood glucose monitoring [15–17], measurement of material

thickness [18], biomedical applications [19], detection of cancerous cells [20], and the evaluation of oils [21]. Metamaterials (MMs) are artificially engineered structures that exhibit negative permeability and permittivity simultaneously [22]. MM designs are often subwavelength structures that are easier to manufacture and have much simpler shapes. MM-based sensing offers enhanced resolution and sensitivity and more flexibility in designing the sensors [23].

The most widely used configuration of MM is the split-ring resonator (SRR) due to its intriguing EM characteristics. The SRR provides a strong magnetic resonance in response to EM excitation when the magnetic energy stored in the inductor and the electrical energy stored in the capacitor is balanced by distance, size, structure, and orientation [24]. Since the last few years, numerous researchers have demonstrated the use of metamaterials as electrochemical sensors. Recent advances in thin-film metamaterials used in therapeutic and diagnostic applications are reviewed in [25]. Microfluidic sensors based on MM are presented in [22], operating from gigahertz to terahertz. A substrate-integrated waveguide sensor for characterising chemicals at millimetre-wave (mm-W) frequency range was presented in [26]. The researchers have proposed various techniques to increase the sensitivity of these sensors by creating a gap between complementary split-ring resonator (CSRR) [27], employing planar microwave resonators [10], and designing closed-loop inside split-ring resonator [17].

A couple of MM-based sensors were reported in [2, 28] to detect branded and unbranded diesel types. In another study, a G-shaped metamaterial absorber based sensor was proposed to detect various oils including corn oil, olive oil, and cotton oil [29]. Most sensors studied have low sensitivity, which can cause difficulties in detecting oils having small changes in dielectric permittivity and loss tangent. The sensor can be manipulated for various MM-W band applications with an appropriate design, leading to smaller sizes and inconsequential response to impurity in the material under test (MUT) and temperature variation [20].

Besides, public health's significance requires a regular check on cooking oil's quality as the consumption of unhealthy oils can lead to deadly diseases. Particularly in developing countries, the awareness of edible oil purchasing choice is relatively lower than in developed regions [30]. To the best of the author's knowledge, no metamaterial-based sensor applicable in oil's characterisation has been proposed yet operating at millimetre-wave (MM-W) frequencies. Therefore, lightweight, smaller, and highly sensitive metamaterial-based split-ring resonator (MM-SRR) could be designed to assess the quality of cooking oils by detecting minor changes in the dielectric constant due to its chemical characteristics.

2. Design of MM-Based Split-Ring Resonator

A grouping of split-ring resonators connected by a microstrip transmission line and a ground structure is considered for the characterisation of oils by calculating their changes in the dielectric constant. The design's novelty lies in the two split rings (one enclosed by the other) and its operation at millimetre-wave frequencies. Rogers 5880 of 0.25 mm thickness having a dielectric constant, $\varepsilon r = 2.2$, and tangent loss, $\tan\theta = 0.0009$, is used as a preferred substrate for above 10 GHz applications frequencies. The transmission line and the ground are made of copper having a thickness of 35 nm. The cross-sectional view of the proposed design is shown in Figure 1, consisting of two circular split-ring patterns with a different radius and inverse split path. The outer ring is connected to Port 1, while the inner ring is connected to Port 2. The inner ring is surrounded by an outer ring that gives the sensor an enhanced coupling effect.

MM-based ring resonator works like a parallel LC circuit whose resonance frequency is defined by equation (1). The effective inductance (L_{eff}) and effective capacitance (C_{eff}) are caused by the circuit that depends on the metamaterial design's dimensions such as the radii (R_1 and R_2), the width of the split rings (w) as well as the substrate's thickness (h) [31]:

$$f_r = \frac{1}{2\pi\sqrt{L_{\text{eff}}C_{\text{eff}}}}. \tag{1}$$

The effective capacitance is the sum of surface capacitance (C_s) and the gap capacitance (C_g), which are represented in equations (2) and (3), respectively [6]:

$$C_g = \varepsilon_0\frac{hw}{g} + \varepsilon_0\left(\frac{2\pi h}{\ln(2.4h/w)}\right), \tag{2}$$

where ε_0 = free-space permittivity.

$$C_s = 2\varepsilon_0\frac{(h)}{\pi}\ln\left(\frac{4R_2}{g}\right). \tag{3}$$

The effective inductance of the resonator is determined using the following equation [31]:

$$L = \frac{\mu_0(R_1 + w/2)}{2\pi}\left(\ln\frac{8(R_2 + w/2)}{h + w} - 0.5\right), \tag{4}$$

where μ_0= free-space permeability.

The parameters h, w, R_1, R_2, and G altogether change the metamaterial resonator's resonant frequency. The required dimensions of the structure were calculated using equations (1)–(4). Through parametric studies, further modifications were done to get the resonance frequency near the desired range. Table 1 shows the optimized dimensions for the designed resonating at 30 GHz.

3. Simulation and Characterisation of the Design

Overall dimensions of the proposed structure were optimized through a parametric study. The numerical study was conducted on the three potential parameters affecting the transmission response of the design. Figures 2–4 show the effect of the width of split rings (L_{r1} and L_{r2}), the radius of outer split-ring (R_2), and the radius of inner split-ring (R_1), respectively, on resonance frequency. It can be noticed that the increase in radii of split rings causes the resonance to move towards lower frequencies. On the other hand, width

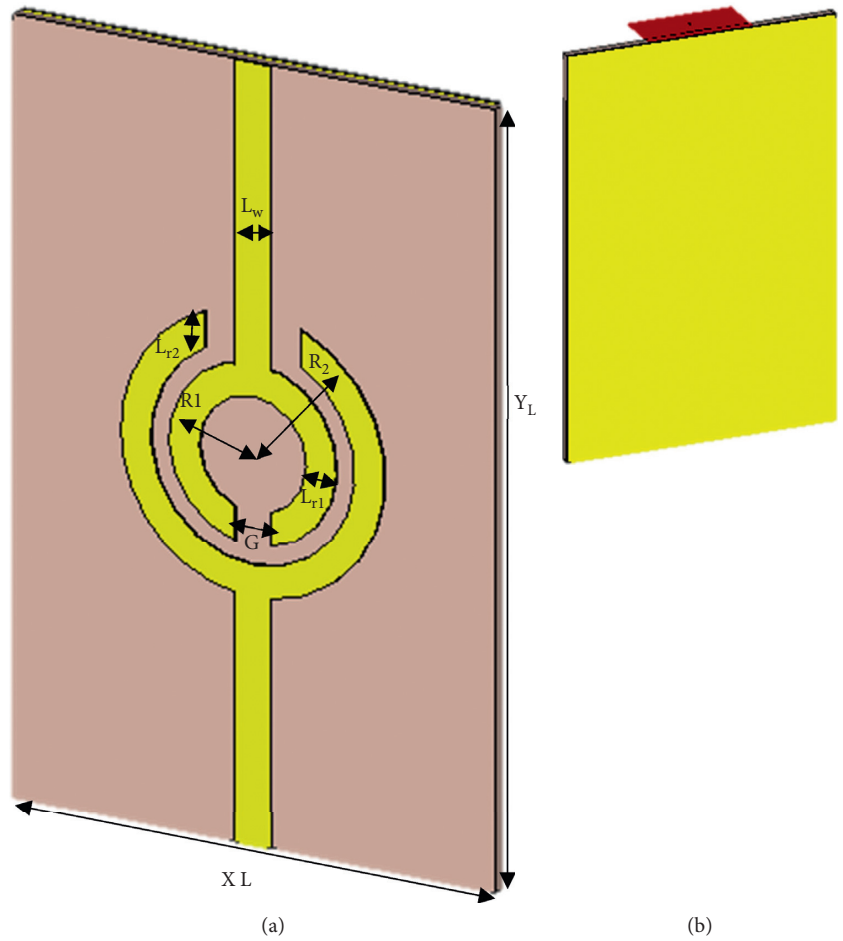

Figure 1: Design of proposed metamaterial-based SRR: (a) top view and (b) bottom view (full ground plane).

Table 1: Dimensions of the split-ring resonator in mm.

Parameter	Value (mm)	Parameter	Value (mm)
X_L	8	Y_L	12
R_1	1.45	R_2	2.5
$w = L_{r1} = L_{r2}$	0.5	G	0.6
L_w	0.6		

shifts the resonance towards higher frequencies due to the lesser gap between the two rings. We have chosen L_{r1} and L_{r2}, 0.5 mm to maintain a sufficient difference between them and avoid the rings overlap over each other.

The highest negative peak is obtained when R_1 is 1.45 mm and R_2 is 2.5 mm.

The proposed design is simulated and optimized using Computer Simulation Technology (CST) microwave studio and MATLAB software for metamaterial characterisation. A Numerical Robust Method (NRM) is used to test the characteristics of the metamaterial using equations (5)–(9) [32]. Figure 5 shows the simulated transmission, S_{21}, and reflection, S_{11}, coefficients, which indicate that the structure resonates at 30 GHz (S_{21}). However, the reflection coefficient, S_{11}, at the resonance frequency, is found to be close to zero. As seen in Figure 6 at the negative peak of S_{21}, effective permittivity, ε_r, becomes negative and stays negative at 29 to

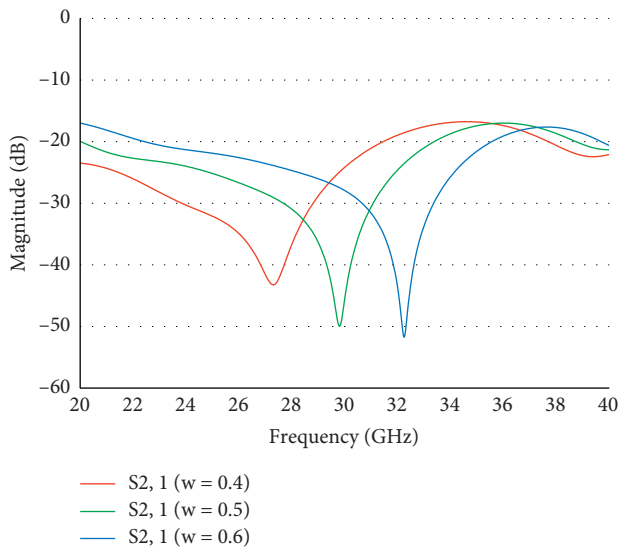

Figure 2: Effect of the "w" on resonance.

31 GHz (highlighted in blue). Besides, permeability, μ is negative from 22 GHz to 32 GHz, and a transition from positive to negative is observed in the refractive index, n, precisely at the resonance frequency (30 GHz). Metamaterial

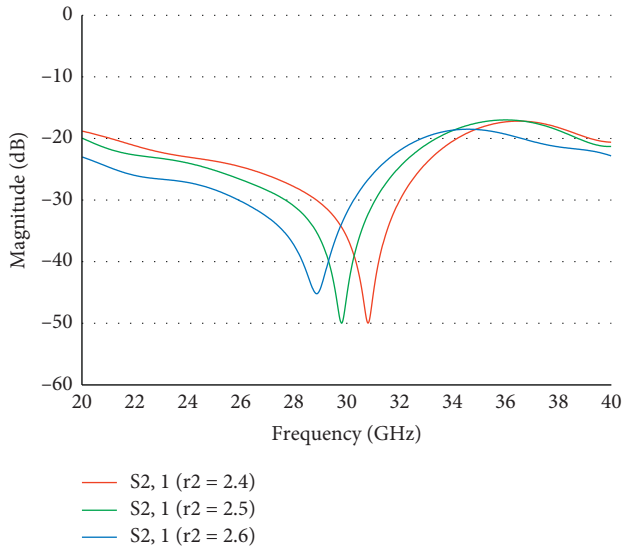

Figure 3: Effect of "R_2" on resonance.

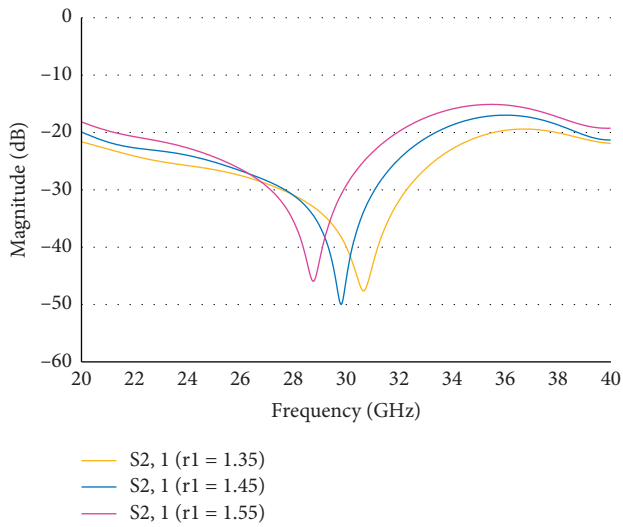

Figure 4: Effect of the "R_1" on resonance.

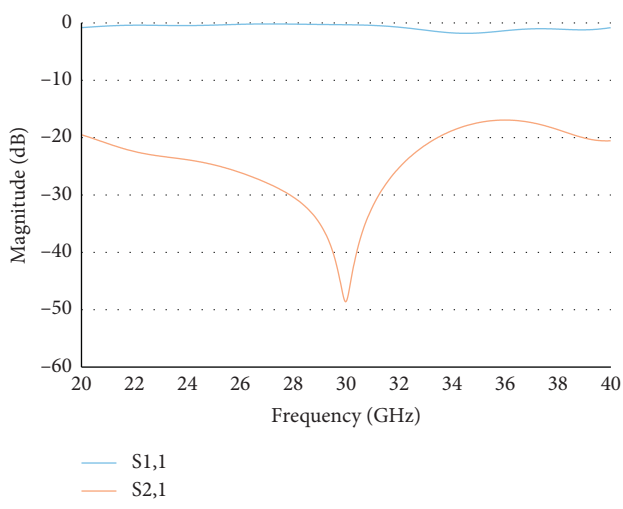

Figure 5: S-parameters of the designed SRR.

exhibiting double negative (DNG) characteristics is represented in a bandwidth of 30 GHz to 31 GHz where all parameters (ε, μ, and n) had a negative value in this range of frequencies:

$$n = \frac{1}{k_0 d}\left\{\left[\left[\ln\left(e^{\mathrm{ink}_0 d}\right)\right]'' + 2m\pi\right]i\left[\ln\left(e^{\mathrm{ink}_0 d}\right)\right]'\right\}, \tag{5}$$

where

$$e^{\mathrm{ink}_0 d} = X \pm i\sqrt{1 - X^2}, \tag{6}$$

$$X = \frac{1}{2S_{21}\left(1 - S_{11}^2 + S_{21}^2\right)}. \tag{7}$$

Here, m is associated with the branch index (n') whose real part is represented by (') and the imaginary part is represented by ("):

$$\varepsilon = \frac{n}{z}, \tag{8}$$

$$\mu = nz. \tag{9}$$

On the other hand, physical characterisation for the designed resonator is described by the electric field and surface current distribution. The resultant electric field distributions due to Port 1 and Port 2 on the resonator are illustrated in Figures 7(a) and 7(b), respectively, for the resonance frequency. It can be seen in Figure 7 that the electric field distributes evenly to the sides of the split ring by the impact of gaps between the outer and inner ring, which is visible at the sides of the outer ring. Moreover, it can be seen that electric field distribution for the outer ring is weaker than the inner ring emphasising that the inner ring is the central entity responsible for the resonance frequency. The electric field's high intensity can be seen at the resonance frequency near the gap of the inner split ring and both copper rings, which represents the most sensitive area to the dielectric changes.

As shown in Figures 8(a) and 8(b), the surface current illustrates that the surface current's clockwise direction is dominant in the inner ring, while the counterclockwise direction is dominant in the outer ring. The strength of the resultant surface current at the inner ring's sides is comparatively higher than that of the outer ring at the resonance frequency of 30 GHz. Similar to electric field distribution, it can be seen from the surface current distributions that the inner ring is mainly responsible for the resonance frequency.

4. Validation of Sensor

In this section, performance and sensitivity analysis is carried out on the designed sensor by realising the perturbation phenomenon, which leads to the change in quality factor and shift in the resonance frequency. The magnetic field's stored energy is typically equal to the energy stored due to the electric field at the resonance frequency. Conversely, the magnetic and electric fields form a new resonance by altering the material under test (MUT) insertion on or near the resonator depending on the variation in permittivity, permeability, and MUT

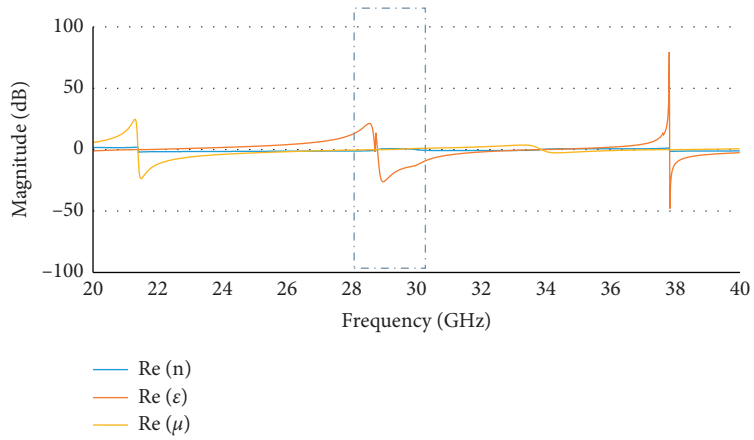

Figure 6: Metamaterial characterisation of the proposed SRR.

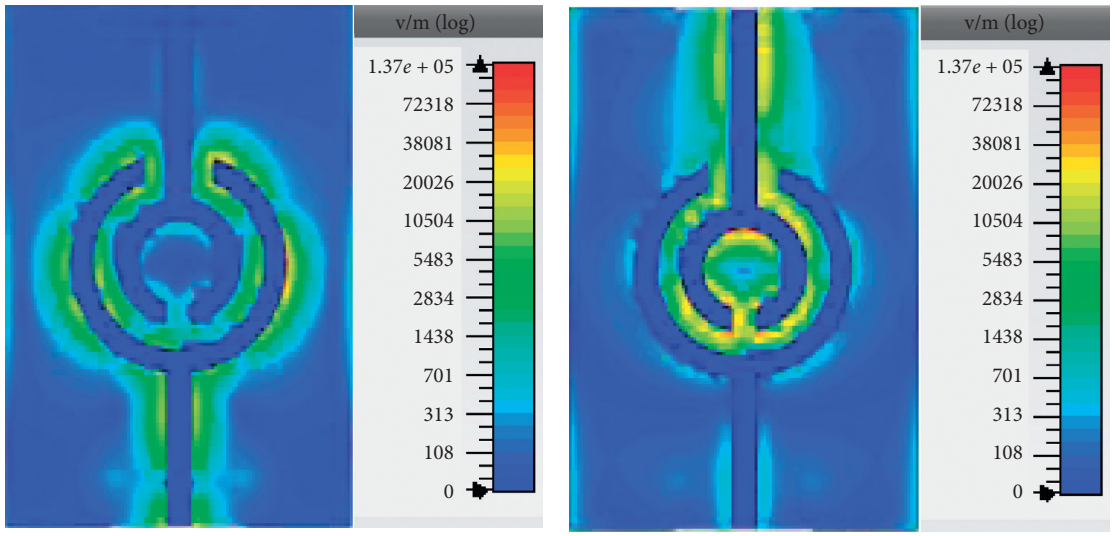

(a) (b)

Figure 7: Electric field distribution at 30 GHz due to (a) Port 1 and (b) Port 2.

volume [33]. In this study, the MUT was introduced on the sensor covering its entire surface, as shown in Figure 9, where MUT can be termed as an overlayer.

4.1. Impact of Sample Volume. Initially, the impact of the thickness of MUT on resonance was analysed by keeping the dielectric value constant at 2.454 (near the range of oils' dielectric values) and varying its volume. It was done to find the minimum thickness sufficient to mitigate the sensor's cross-sensitivity to sample volume. Figure 10 shows the percentage shift in resonance frequency when the MUT thickness is increased from 0.8 mm to 1.6 mm. It can be demonstrated that when the thickness is increased above 0.8, the percentage shift in the resonance frequency is lower than 0.2. Therefore, the suitability of the sensor can be determined as an instrument distinguishing the dielectric properties of MUT regardless of its volume.

In order to test the applicability of the sensor for oil chemical characterisation purposes, the sensor was investigated with the existence of the 5 mm thickness of MUT having different dielectric constants. The dielectric constants of castor oil, olive oil, tallow, corn oil, soybean salad oil, and conventionally rendered bacon fat were considered in simulation [34, 35]. The dielectric constant in oils is typically influenced by temperature and chemical characteristics such as oils' moisture contents. The dielectric properties and chemical characteristics (iodine contents, moisture and volatile ratio, and solid-fat index values) of the six oils considered in this study are represented in Table 2.

Figure 11 depicts that, with the increase in dielectric constant, the resonance frequency shifted to the left side (lower frequencies) and demonstrated that a larger dielectric value causes a larger shift in the resonance frequency dip. Six types of oils were used to analyse the sensor's sensitivity that caused the realisation of perturbation in the sensor's transmission coefficient (S_{21}). The resonance frequency of

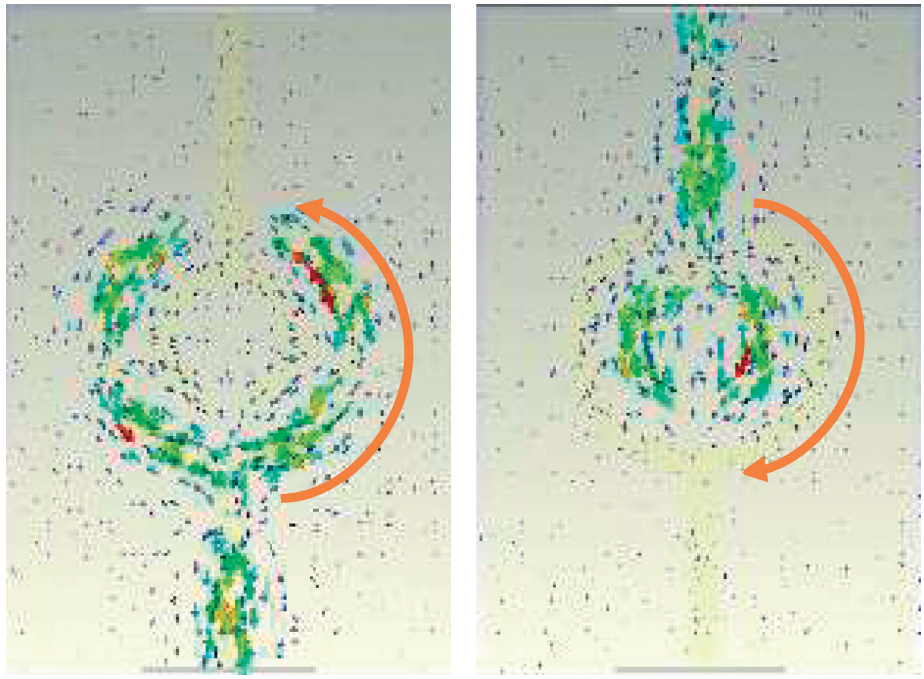

(a) (b)

Figure 8: Surface current distribution due to (a) Port 1 and (b) Port 2.

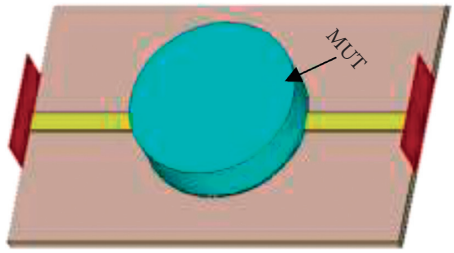

Figure 9: Placement of MUT on the surface of the sensor.

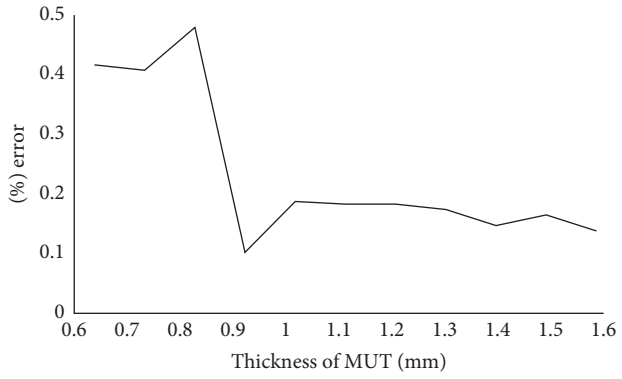

Figure 10: The percentage error in resonance shift versus thickness of MUT.

the sensor on the smallest value of dielectric constant occurred at 35.5 GHz (above resonance frequency) due to the comparatively large volume sample with a low value of permittivity and loss tangent.

Nevertheless, a significant shift in resonance frequency can be observed. There is a difference of 0.94 GHz seen in the resonance frequencies of bacon fat and tallow, and 2.11 GHz between olive oil and tallow's resonances.

For further assessment, the transmission coefficient's phase is used to distinguish the oil's properties. The characteristics of a metamaterial can be demonstrated with the transition in phase at the resonance frequency. Similar to prior investigations, the impact of the MUT's thickness was also analysed. The phase transition is depicted in Figure 12, where distinct shifts are noticeable inside the red-box in the frequency range of 28 to 37 GHz for castor oil, olive oil, tallow, corn oil, soybean salad oil, and conventionally rendered bacon fat. On the other hand, there is a shallow difference found in the negative peak of resonance frequencies for corn oil and soybean salad oil due to their almost similar dielectric properties.

Figure 13 represents the percentage error in the transition of the shift in the transmission coefficient phase when MUT thickness is increased. It is validated that overlayer thickness provides less percentage error shift in the phase transition than the percentage error shift in the resonance frequency. According to these simulations, the proposed structure can be used in investigations of various oils. The proposed model can detect the low values of the dielectric constant regardless of the thickness of the samples.

4.2. Sensitivity Analysis. This part of the study explores the sensitivity of the metamaterial-based sensor in dielectric characterisations. The sensitivity analysis is calculated based on the results from full-wave electromagnetic simulations.

Table 2: Chemical and dielectric properties of some commercial oils [34–36].

Oil name	Iodine contents	Moisture and volatiles (%)	Relative dielectric constant (ε_r')	Loss tangent (tan δ)	Solid-fat index
Bacon fat	171 (gI_2/100g)	0.06	2.5	0.0532	23.6
Tallow	45 (gI_2/100g)	0.075	2.430	0.0485	26.3
Castor oil	85 (gI_2/100g)	0.2	4.47	0.0322	97.5
Olive oil	84 (gI_2/100g)	0.2	3.254	0.0331	20
Soybean salad oil	121 (gI_2/100g)	0.04	2.506	0.0539	None
Corn oil	110 (gI_2/100g)	0.32	2.526	0.0566	None

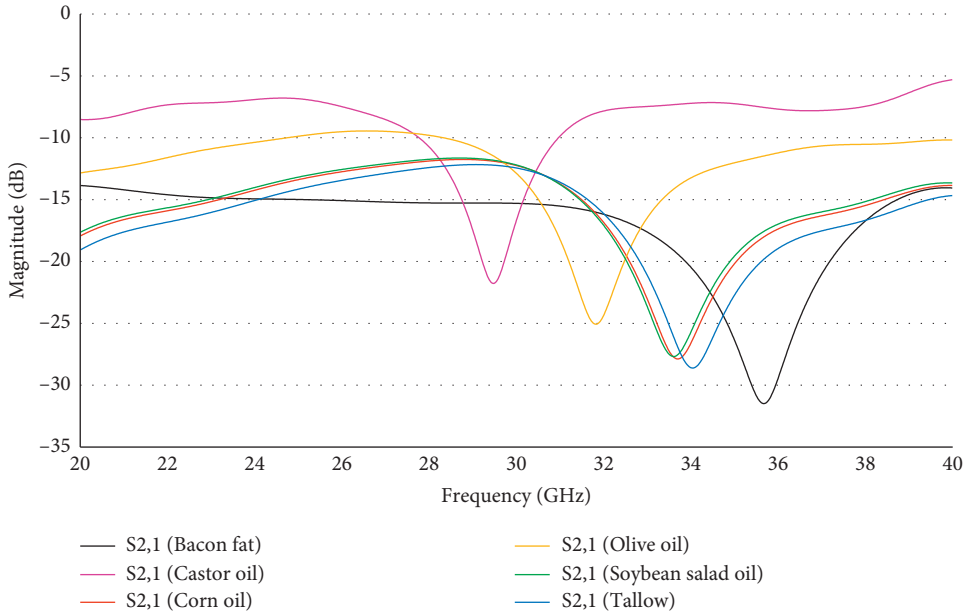

Figure 11: Perturbation in resonance frequency under MUT.

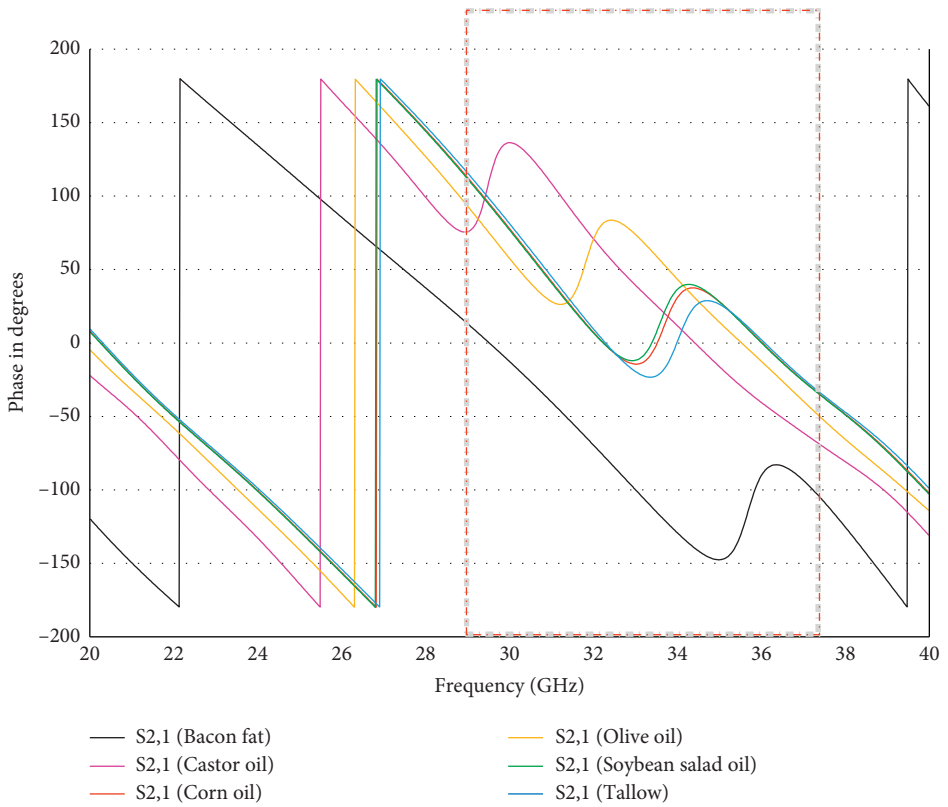

Figure 12: The shift in the transition of phase under MUT on different cooking oils at the resonance frequency.

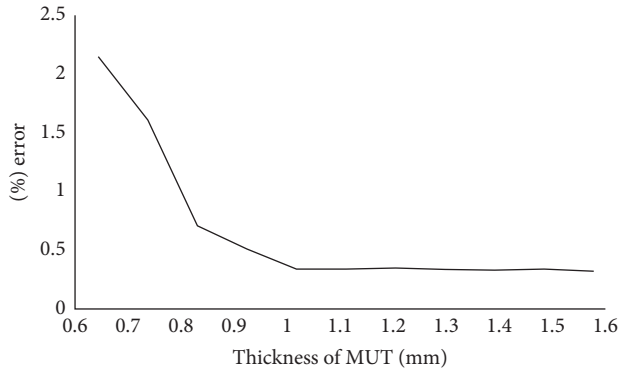

Figure 13: The percentages error in phase shift versus thickness of MUT.

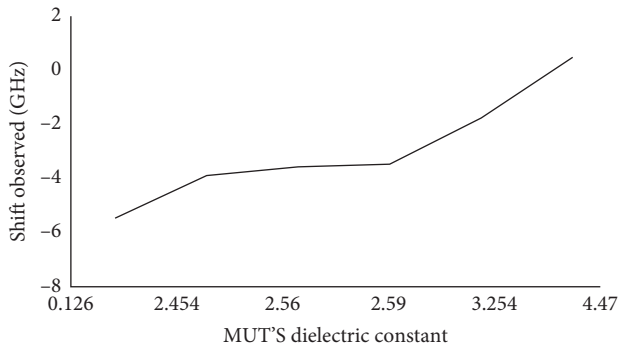

Figure 14: Sensitivity chart according to the dielectric constants.

When an oil sample is placed over the sensor's surface, the shift in the negative peak of resonance frequency can be observed. The resonance frequency shift can be defined mathematically as in equation (10), where f_r is the resonance frequency due to the MUT introduced and α is the resonance frequency without any sample, while f_s is the difference between the new and original notch frequencies (shifted frequency) [37]:

$$f_s = f_r - \alpha. \tag{10}$$

By taking into account the differences in the highest and lowest dielectric constants of the materials under tests and respective frequency shifts observed, the sensitivity can be calculated using [37]

$$S = \lim_{\Delta(\varepsilon_h - \varepsilon_l) \longrightarrow 0} \frac{\Delta f_{sh} - \Delta f_{sl}}{\Delta \varepsilon_h - \Delta \varepsilon_l}. \tag{11}$$

In equation (11), f_{sh} and f_{sl} represent the frequency shift on the placement of MUT with the highest and lowest dielectric constant, respectively, whereas ε_h represents the highest dielectric constant and lowest dielectric constant considered in this study is represented by ε_l since the highest and lowest value of dielectric constant exhibited by the MUTs considered in this study is 4.47 and 0.126, respectively.

Therefore, the calculated sensitivity for the designed sensor is 1.12 GHz per unit change in dielectric constant as shown in Figure 14. The sensitivity graph depicts that the trend is approximately linear with the rise in dielectric constant according to the frequency shifts. It is worth recalling that the sample's dielectric constant assumed here is the maximum value, which occurs at the equilibrium between the electrical field and the molecular orientation [34]. Another point to remember is that each oil contains several fatty acids that differ in relative percentages depending on the type and origin of the oil; hence, a logical assessment essential to pure fatty acids and pure acids cannot be carried out easily. Despite that, there is a minimal difference in dielectric constants' magnitude between the values observed under various temperature and frequency conditions.

Nevertheless, working in the millimetre-wave contributes to tackling this issue as it is insignificantly affected by the temperature variations. Besides, mm-wave also offers a higher sensitivity to the minimal changes in the dielectric constant of oils according to the differing proportions of fatty acids and pure acids. Thus, the designed sensor can be assumed to be a promising candidate in sensing the chemical characteristics of oil based on the contents that vary its dielectric characteristics.

Table 3 describes the sensitivity of the designed sensor for the characterisation of oils compared to the previously designed sensors. The results based on a shift in resonance frequency often display a better accuracy for low values of dielectric constants. However, the accuracy in the designed resonator increases as the value of the dielectric constant decreases. This makes the mm-wave more sensitive to the

Table 3: Comparison with the other designed resonators.

Reference	Sensor design	Method of sensing	Operating frequency (GHz)	Sensitivity (GHz)	Application
[26]	SIW	S_{11}	16	0.14	Chemical
[27]	CSRR	S_{21}	2.3	0.1	Alcohol
[10]	PSRR	S_{21}	1.9	0.2	Bacterial growth
[28]	Omega	S_{21}	2	0.05	Methanol
[38]	CSRR resonator	S_{11}	2.5	0.5	Glucose
[39]	M-CRR	S_{21}	2.4	0.06	Liquids
[40]	PMWR	S_{21}	1.5	0.01	Liquids
This study	MM-SRR	S_{21}	30	1.12	Oils

dielectric changes, which is the key to the designed sensor's relatively enhanced efficiency.

5. Conclusion

This study focuses on designing the metamaterial-based split-ring resonator to detect oils and their chemical characteristics. The sensing characteristics of the proposed sensing structure are provided using the transmission coefficient and its phase. The sensor's sensitivity from the results can be estimated to be 1.12 GHz per unit increase in the dielectric constant. The design's benefits and efficiency are significant for identifying minimal changes in the sample's dielectric constant regardless of the sample's volume and impurities and temperature variations. A significant shift in the transmission coefficient (amplitude and phase) behaviour and linearity of sensing offer a novel sensing mechanism vital for other liquid-sensing applications, such as blood and water.

Data Availability

The corresponding author can be contacted for any related data.

Conflicts of Interest

The authors declare no conflicts of interest.

Acknowledgments

The authors would like to thank the Ministry of Higher Education Malaysia (MOHE) for supporting this research under Fundamental Research Grant Scheme Vot no. FRGS/1/2019/TK04/UTHM/02/13 and it is partially sponsored by Universiti Tun Hussein Onn Malaysia.

References

[1] M. Erdoğan, E. Ünal, F. Özkan Alkurt, Y. I. Abdulkarim, L. Deng, and M. Karaaslan, "Determination of frying sunflower oil usage time for local potato samples by using microwave transmission line based sensors," *Journal of the International Measurement Confederation*, vol. 163, Article ID 108040, 2020.

[2] A. Tamer, F. Karadağ, E. Ünal et al., "Metamaterial based sensor integrating transmission line for detection of branded and unbranded diesel fuel," *Chemical Physics Letters*, vol. 742, Article ID 137169, 2020.

[3] A. Salim, S.-H. Kim, J. Y. Park, and S. Lim, "Microfluidic biosensor based on microwave substrate-integrated waveguide cavity resonator," *Journal of Sensors*, vol. 201813 pages, 2018.

[4] Z. Wei, "A high-sensitivity microfluidic sensor based on a substrate integrated waveguide Re-entrant cavity for complex permittivity measurement of liquids," *Sensors*, vol. 18, no. 11, Article ID 4005, 2018.

[5] Y. Abdulkarim, L. Deng, M. Karaaslan et al., "The detection of chemical materials with a metamaterial-based sensor incorporating oval wing resonators," *Electronics*, vol. 9, no. 5, p. 825, 2020.

[6] H. Torun, F. Cagri Top, G. Dundar, and A. D. Yalcinkaya, "An antenna-coupled split-ring resonator for biosensing," *Journal of Applied Physics*, vol. 116, no. 12, Article ID 124701, 2014.

[7] M. N. Hasan, S. Tamanna, P. Singh, M. D. Nadeem, and M. Rudramuni, "Cylindrical dielectric resonator antenna sensor for non-Invasive glucose sensing application," ", in *Proceedings of the 2019 6th International Conference On Signal Processing And Integrated Networks*, pp. 961–964, Noida, India, March 2019.

[8] H. Saghlatoon, R. Mirzavand, M. M. Honari, and P. Mousavi, "Sensor antenna transmitter system for material detection in wireless-sensor-node applications," *IEEE Sensors Journal*, vol. 18, no. 21, p. 8812, 2018.

[9] A. Taeb, M. A. Basha, S. Gigoyan, M. Marsden, and S. Safavi-Naeini, "Label-free DNA sensing using millimeter-wave silicon WGM resonator," *Optics Express*, vol. 21, no. 17, Article ID 19467, 2013.

[10] S. Mohammadi, A. V. Nadaraja, K. Luckasavitch, M. C. Jain, D. J. Roberts, and M. H. Zarifi, "A label-free, non-intrusive, and rapid monitoring of bacterial growth on solid medium using microwave biosensor," *IEEE Transactions on Biomedical Circuits and Systems*, vol. 14, no. 1, pp. 2–11, 2020.

[11] F. Foroutan and N. K. Nikolova, "UWB active antenna for microwave breast imaging sensing arrays," *IEEE Antennas and Wireless Propagation Letters*, vol. 18, no. 10, 2019.

[12] A. Soffiatti, Y. Max, S. G. Silva, and L. M. De Mendonça, "Microwave metamaterial-based sensor for dielectric characterization of liquids," *Sensors*, vol. 18, no. 5, p. 1513, 2018.

[13] A. Sadeqi and S. Sonkusale, "Low-cost metamaterial-on-paper chemical sensor," in *Proceedings of the TRANSDUCERS 2017 - 19th International Conference On Solid-State Sensors*, pp. 1437–1440, Actuators and Microsystems, Kaohsiung, Taiwan, June 2017.

[14] T. U. Haq, C. Ruan, X. Zhang, and S. Ullah, "Complementary metamaterial sensor for nondestructive evaluation of dielectric substrates," *Sensors*, vol. 19, no. 9, p. 2100, 2019.

[15] J. Vrba and D. Vrba, "A microwave metamaterial inspired sensor for non-invasive blood glucose monitoring," *Radioengineering*, vol. 24, no. 4, p. 877, 2015.

[16] A. E. Omer, G. Shaker, S. Safavi-Naeini et al., "Multiple-cell microfluidic dielectric resonator for liquid sensing applications," *IEEE Sensors Journal*, vol. 21, no. 5, p. 6094, 2021.

[17] A. Kandwal, T. Igbe, J. Li et al., "Highly sensitive closed loop enclosed split ring biosensor with high field confinement for aqueous and blood-glucose measurements," *Scientific Reports*, vol. 10, no. 1, p. 4081, 2020.

[18] M. Islam, M. Rahman, M. Samsuzzaman, M. Mansor, and N. Misran, "Resonator-inspired metamaterial sensor: design and experimental validation for measuring thickness of multilayered structures," *Sensors*, vol. 18, no. 12, Article ID 4213, 2018.

[19] B. Tutuncu, 2020 Metamaterial Biosensor for ISM Band Biomedical Applications,.

[20] L. La Spada, F. Bilotti, and L. Vegni, "Metamaterial biosensor for cancer detection," in *Proceedings of the Ieee Sensors Proceedings*, pp. 627–630, Limerick, Ireland, October 2011.

[21] N. K. Tiwari, S. P. Singh, and M. J. Akhtar, "Novel improved sensitivity planar microwave probe for adulteration detection in edible oils," *IEEE Microwave and Wireless Components Letters*, vol. 29, no. 2, pp. 164–166, 2019.

[22] A. Salim and S. Lim, "Review of recent metamaterial microfluidic sensors," *Sensors*, vol. 18, no. 1, p. 232, 2018.

[23] M. Bakır et al., "Metamaterials: definitions, properties, applications, and FDTD-based modeling and simulation (Invited paper)," *IEEE Sensors Journal*, vol. 20, no. 1, pp. 1–4, 2020.

[24] S. Gamouh and A. Chaabi, "Microwave biosensor based on a double metamaterial particle," in *Proceedings of the 4th International Conference on Control Engineering and Information Technology*, pp. 1–4, Hammamet, Tunisia, December 2017.

[25] S. RoyChoudhury, V. Rawat, A. H. Jalal, S. N. Kale, and S. Bhansali, "Recent advances in metamaterial split-ring-resonator circuits as biosensors and therapeutic agents," *Biosensors and Bioelectronics*, vol. 86, pp. 595–608, 2016.

[26] M. Memon and S. Lim, "Microwave chemical sensor using substrate-integrated-waveguide cavity," *Sensors*, vol. 16, no. 11, 11 pages, Article ID 1829, 2016.

[27] E. L. Chuma, Y. Iano, G. Fontgalland, and L. L. Bravo Roger, "Microwave sensor for liquid dielectric characterization based on metamaterial complementary split ring resonator," *IEEE Sensors Journal*, vol. 18, no. 24, p. 9978, 2018.

[28] Y. Abdulkarim, L. Deng, M. Karaaslan et al., "Novel metamaterials-based hypersensitized liquid sensor integrating omega-shaped resonator with microstrip transmission line," *Sensors*, vol. 20, no. 3, p. 943, 2020.

[29] Y. I. Abdulkarim, L. Deng, H. Luo et al., "Design and study of a metamaterial based sensor for the application of liquid chemicals detection," *Journal of Materials Research and Technology*, vol. 9, no. 5, pp. 10291–10304, 2020.

[30] Y. A. Negash, D. E. Amare, B. D. Bitew, and H. Dagne, "Assessment of quality of edible vegetable oils accessed in Gondar City, Northwest Ethiopia," *BMC Research Notes*, vol. 12, no. 1, 2019.

[31] M. Asad, S. Al Neyadi, O. Al Aidaros, M. Khalil, and M. Hussein, "Single port bio-sensor design using metamaterial split ring resonator," in *Proceedings of the International Conference On Electronic Devices, Systems, and Applications*, pp. 1–4, Kuching, Malaysia, August 2017.

[32] B. Panzner, M. Anis, A. Jöstingmeier, and A. Omar, ""A numerically robust method for determination of dielectric material parameters," in *Proceedings of the European Microwave Conference*, pp. 1599–1602, Rome, Italy, October 2009.

[33] T. Haq, C. Ruan, S. Ullah, and A. Kosar Fahad, "Dual notch microwave sensors based on complementary metamaterial resonators," *IEEE Access*, vol. 7, Article ID 153489, 2019.

[34] W. E. Pace, W. B. Westphal, and S. A. Goldblith, "Dielectric properties of commercial cooking oils," *Journal of Food Science*, vol. 33, no. 1, pp. 30–36, 1968.

[35] Z. H. Shah and Q. A. Tahir, "Dielectric properties of vegetable oils," *Journal of Scientific Research*, vol. 3, no. 3, pp. 481–492, 2011.

[36] H. Górska-Warsewicz, K. Rejman, W. Laskowski, and M. Czeczotko, "Butter, margarine, vegetable oils, and olive oil in the average polish diet," *Nutrients*, vol. 11, no. 12, Article ID 2935, 2019.

[37] S. K. Yee, S. C. J. Lim, P. S. Pong, and S. H. Dahlan, "Microstrip defected ground structure for determination of blood glucose concentration," *Progress In Electromagnetics Research C*, vol. 99, p. 35, 2020.

[38] A. Ebrahimi, J. Scott, and K. Ghorbani, "Differential sensors using microstrip lines loaded with two split-ring resonators," *IEEE Sensors Journal*, vol. 18, no. 14, pp. 5786–5793, 2018.

[39] A. Ebrahimi, J. Scott, and K. Ghorbani, "Microwave reflective biosensor for glucose level detection in aqueous solutions," *Sensors and Actuators A: Physical*, vol. 301, Article ID 111662, 2020.

[40] M. H. Zarifi and M. Daneshmand, "Liquid sensing in aquatic environment using high quality planar microwave resonator," *Sensors and Actuators B: Chemical*, vol. 225, pp. 517–521, 2016.